



Tunable Luminescence of CeAl₁₁O₁₈ Based Phosphors by Replacement of (AlO)⁺ by (SiN)⁺ and Co-Doping with Eu

Liang-Jun Yin,^a Guo-Zhang Chen,^a Chao Wang,^{a,z} Xin Xu,^{b,z} Lu-Yuan Hao,^b and Hubertus T. (Bert) Hintzen^c

^aSchool of Energy Science and Engineering, University of Electronic Science and Technology of China, Chengdu, People's Republic of China

^bLaboratory of Materials for Energy Conversion, Department of Materials Science and Engineering, University of Science and Technology of China, Hefei, People's Republic of China

^cLuminescent Materials Research Group, Faculty of Applied Sciences, Delft University of Technology, JB Delft 2629, The Netherlands

A series of Si-N or Eu-Li doped CeAl₁₁O₁₈ and CeAl₁₂O₁₈N phosphors are prepared by solid-state reaction. Their structure and luminescence are researched carefully. Si-N doping with the concentration less than 8% can be successfully dissolved into CeAl₁₁O₁₈ crystal lattice and doesn't change the matrix structure, only resulting in crystal lattice shrinkage due to the shorter bond length for Si-N bond versus Al-O bond. It is observed that blue emission gradually decreases and UV emission becomes stronger due to the gradual disappearance of O_{Me} ions with the increase of Si-N doping. Compared with the traditional UV emitting phosphor CeMgAl₁₁O₁₉, Si-N doped CeAl₁₁O₁₈ shows better thermal stability. The crystal structure and lattice parameters of Eu-Li codoped CeAl₁₁O₁₈ remain unchanged due to the large tolerance of rare-earth sites. On account of the energy transfer from UV emission of Ce³⁺ to Eu²⁺, a single overlapping blue emission with high intensity is obtained in Eu-Li codoped CeAl₁₁O₁₈ phosphor. © 2014 The Electrochemical Society. [DOI: 10.1149/2.0191407jss] All rights reserved.

Manuscript submitted April 22, 2014; revised manuscript received May 27, 2014. Published June 20, 2014.

In recent years, rare-earth doped aluminates with hexagonal structure such as BaMgAl₁₀O₁₇:Eu²⁺, CaAl₁₂O₁₉:M (M = Eu, Mn), LaMgAl₁₁O₁₉:Ce³⁺ have been used as energy conversion phosphors for fluorescent lamps, LED or PDP displays.¹⁻⁷ These phosphors show some features of high quantum yield, chemical and radiation stability, which make them still under research in many areas now. It is demonstrated here that some aluminates will show very interesting results by tuning the crystal structure slightly, despite (oxy)nitride based phosphors are researched widely and greatly developed recently due to their high quantum efficiency, excellent thermal, physical and chemical stabilities, and therefore show large potential to be implemented in highly efficient and reliable white LEDs.⁸⁻¹⁰

Generally, the hexagonal aluminates are divided into three different groups:¹¹⁻¹³ 1. compounds MeAl₁₂O₁₉ (Me = Ca, Sr, Eu) with magnetoplumbite-type structure; 2. compounds MeMgAl₁₀O₁₇ (Me = Ba, Sr, Eu) with β -alumina structure; 3. distorted magnetoplumbite-type structure such as CeAl₁₁O₁₈. The β -alumina structures and magnetoplumbite are both composed of spinel blocks formed by the close packing of Al and O atoms. There is the merely significant difference in the two mirror planes ($z = 0.25$ and 0.75) between these two structures. In the β -alumina structure, each mirror plane contains one large cation and one oxygen. The non-close-packed mirror plane is connected with the stable spinel blocks closely. In the magnetoplumbite structure, the mirror planes contain one large cation and more oxygens. Generally, CeAl₁₁O₁₈ is considered to have distorted magnetoplumbite structure. The difference from the normal magnetoplumbite-type structure is that La (Ce) large ions are considered to be partially replaced by O ions, O_{Me} as an abbreviation.¹¹ O_{Me} is present because of non-ideal stoichiometry of CeAl₁₁O₁₈ with respect to the ideal MeAl₁₂O₁₉ composition for magnetoplumbite structure (large-cation/small-cation/anion = 1/12/19). Just due to this disorder, CeAl₁₁O₁₈ exhibits special luminescence properties, which will be discussed later.

Within those hexagonal aluminates, as a kind of self-activated phosphor, CeAl₁₁O₁₈ shows very interesting characteristics, i.e. two emission peaks one UV band at ~ 350 nm and one main blue band at ~ 460 nm respectively. As we know, UV light can kill bacteria effectively and blue light is essential in photosynthesis for green plant. Due to its special luminescence properties, CeAl₁₁O₁₈ based phosphors have been applied in sterilization, therapeutic, cosmetic skin treatment and promoting plant growth in greenhouse.¹⁴ To meet the

different requirements in every occasion, the luminescence spectrum must be tunable easily. For example, a narrow UV emission peak can be obtained by substitution La, Y, Sr, Ca large ions for Ce ions or Mg ions for Al ions, whereas the blue emission is largely suppressed in previous study.^{11,14-17}

In this paper, another extremely different method to tune the luminescence spectrum of CeAl₁₁O₁₈ phosphor is carried out by replacing Si-N for Al-O bond or Eu for Ce ions. The luminescence can be arbitrarily designed from blue to UV or UV to blue. It is also found that Si-N doped CeAl₁₁O₁₈ phosphor possesses a better thermal stability, compared with undoped CeAl₁₁O₁₈ phosphor.

Experimental

Synthesis.— The powders with the composition of CeAl_{11(1-x)}Si_{11x}O_{18-11x}N_{11x} ($0 \leq x \leq 0.15$) and Ce_{1-x}Eu_xLi_xAl₁₁O₁₈ ($0 \leq x \leq 0.1$) were prepared by direct solid state reaction under 1 atm flowing N₂ atmosphere. X represents the amounts of Si-N substitution for Al-O bond and Eu substitution for Ce ions respectively. The powder mixtures of Al₂O₃ (99.99 wt%, 100 nm, Wanjing New Material Co. Ltd, Hangzhou, China), CeO₂ (99.9 wt%, Sinopharm Chemical Reagent Co. Ltd, Shanghai, China), Eu₂O₃ (99.99 wt%, Sinopharm Chemical Reagent Co. Ltd, Shanghai, China), Si₃N₄ (96.0%, UBE Industries, Ltd, Japan.), SiO₂ (Sinopharm Chemical Reagent Co. Ltd, Shanghai, China, 99.99%), Li₂CO₃ (Sinopharm Chemical Reagent Co. Ltd, Shanghai, China, 99.99%) were mixed fully in a Si₃N₄ mortar by hand. Stoichiometric raw powders were put into BN crucibles and fired at a temperature 1700°C for 2 h in flowing nitrogen gas. The powder was heated at a constant rate of 300°C/h and cooled down naturally.

Characterization.— The phase formation was analyzed by an X-ray diffractometer (Model PW 1700, Philips Research Laboratories, Eindhoven, The Netherlands) using Cu K α radiation at a scanning rate of 0.5 degree/min. The lattice parameters of CeAl₁₁O₁₈ are calculated by Unit Cell software based on XRD peaks. Energy-dispersed spectroscopy (EDS) measurements were performed at room temperature in a scanning electron microscope (JSM-6390LA, JEOL, Japan). Fourier-Transform Infrared Spectra (FTIR) were recorded at room temperature on a spectrophotometer (Model EQUINOX 55, Bruker, Karlsruhe, Germany) in the range of 500–2000 cm⁻¹. 1 mg of powder was mixed with KBr for dispersion and then pressed into transparent sheet. The electron density calculations were performed using the CASTEP code.¹⁸⁻²⁰ A plane wave basis set with kinetic energy cutoff

^zE-mail: cwang@uestc.edu.cn; xuxin@ustc.edu.cn

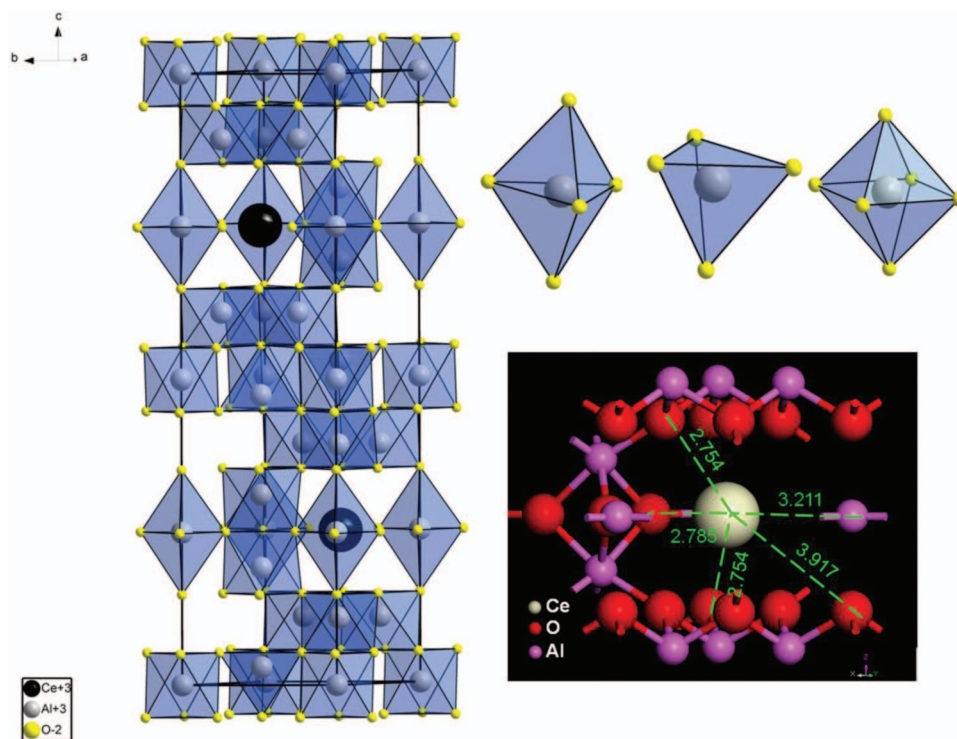


Figure 1. Crystal structure of $\text{CeAl}_{11}\text{O}_{18}$ and local structure around Ce^{3+} ions.

at 500 eV was employed, and the Perdew-Burke-Ernzerhof form^{21–23} of the generalized gradient approximation (GGA) was used to describe the exchange-correlation interactions, while the electron-ion interaction was accounted for through the use of ultrasoft pseudopotentials. The detailed parameters were chosen as follows: k-point spacing = 0.067 \AA^{-1} , sets of k points = $1 \times 1 \times 1$, space representation = reciprocal, and SCF tolerance threshold = $1.0 \times 10^{-5} \text{ eV/atom}$.

Luminescence Properties.— The photoluminescence spectra were measured at room temperature by a fluorescent spectrophotometer (Model F-4600, Hitachi, Tokyo, Japan) with a 200 W Xe lamp as an excitation source. The emission spectrum was corrected for the spectral response of a monochromator and Hamamatsu R928P photomultiplier tube (Hamamatsu Photonics K.K., Hamamatsu, Japan) by a light diffuser and tungsten lamp (Noma Electric Corp., NY; 10 V, 4 A). The excitation spectrum was also corrected for the spectral distribution of the xenon lamp intensity by measuring Rhodamine-B as reference. The temperature dependent luminescence spectra were recorded in the range of 25°C – 300°C with a 200 W Xe lamp as an excitation source and a Hamamatsu MPCD-7000 multichannel photodetector (Hamamatsu Photonics K.K., Hamamatsu, Japan).

Results and Discussion

$\text{CeAl}_{11}\text{O}_{18}$.— Figure 1 shows the crystal structure of $\text{CeAl}_{11}\text{O}_{18}$.^{11,24} $\text{CeAl}_{11}\text{O}_{18}$ has a similar crystal structure to $\text{LaAl}_{11}\text{O}_{18}$. The $\text{CeAl}_{11}\text{O}_{18}$ structure is drawn from a simultaneous substitution of La^{3+} with Ce^{3+} ions. It is reported to have a magnetoplumbite structure with hexagonal space group $P6_3/mmc$ (No. 194) with the lattice constants $a = 5.5581 \text{ \AA}$ and $c = 22.0121 \text{ \AA}$. It is composed of spinel block and mirror plane. The spinel block is built-up by the $[\text{AlO}_4]$ tetrahedron, $[\text{AlO}_5]$ hexahedron and $[\text{AlO}_6]$ octahedron, which are connected by corner-sharing or edge-sharing. Besides, the space around the Ce^{3+} location is large, making possible substitution by doping other metal cations with large radius.

As seen in Figure 2, at the reaction temperature 1700°C and the holding time 2 h, the starting materials Al_2O_3 and CeO_2 are transferred into the product consisted of major $\text{CeAl}_{11}\text{O}_{18}$ and minor

CeAlO_3 phase. The strong XRD peaks of the powders match well with the standard date (JCPDS card number: 00-048-0055), indicating the $\text{CeAl}_{11}\text{O}_{18}$ phase can be obtained under this synthesis condition. Actually $\text{CeAl}_{11}\text{O}_{18}$ phase can always be synthesized successfully in the synthesis temperature ranged from 1500 to 1700°C . For better crystallinity and luminescence properties, the synthesis temperature of 1700°C is fixed to fire the starting materials and research the structure and luminescence properties of $\text{CeAl}_{11}\text{O}_{18}$.

To research the influence of CeAlO_3 purity on the luminescence properties in the products, CeAlO_3 is prepared. The photoluminescence results show that the influence of CeAlO_3 can be neglected because its luminescence intensity is extremely weak and the amount of CeAlO_3 is too small in the products here. Figure 3 shows the photoluminescence of $\text{CeAl}_{11}\text{O}_{18}$ powders. This phosphor shows two emission peaks at 350 nm (UV band) and 450 nm (blue band) under 260 nm excitation respectively. As we know, for $\text{CeAl}_{11}\text{O}_{18}$ with

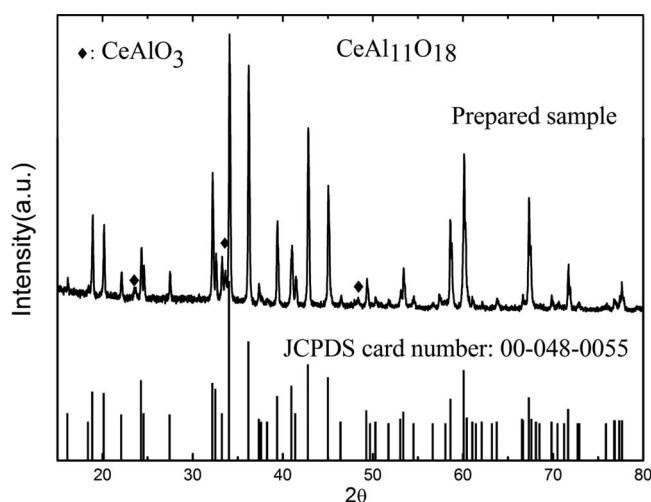


Figure 2. XRD patterns of $\text{CeAl}_{11}\text{O}_{18}$ synthesized at 1700°C for 2h.

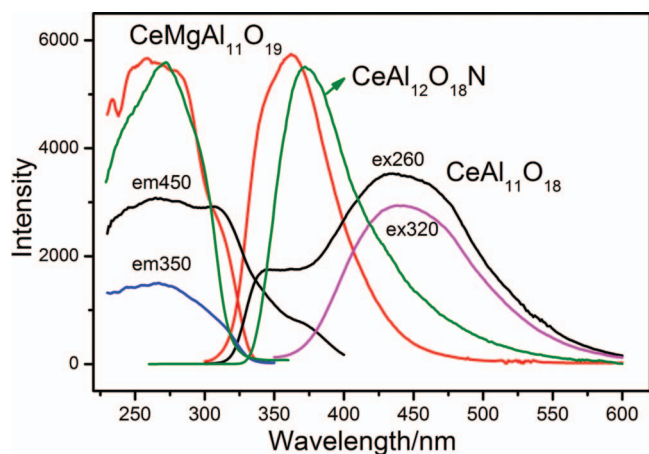


Figure 3. Excitation and emission spectra of $\text{CeAl}_{11}\text{O}_{18}$, $\text{CeMgAl}_{11}\text{O}_{19}$ and $\text{CeAl}_{12}\text{O}_{18}\text{N}$ powders. For $\text{CeAl}_{11}\text{O}_{18}$, the value in the inset represents the corresponding monitored emission wavelength and excitation wavelength.

disordered magnetoplumbite-type structure, Ce ions are replaced by O ions partly, named as O_{Me} for short. It is commonly believed that the UV emission is ascribed to 4f-5d electron transitions of normal Ce^{3+} in $\text{CeAl}_{11}\text{O}_{18}$ crystal lattice, whereas the blue emission is ascribed to Ce- O_{Me} associates.¹¹ This blue emission shouldn't come from Ce- O_{Me} charge transfer transitions because generally these charge transfer transitions happen at very higher energy. The 5d-4f emission of Ce^{3+} coordinated with O_{Me} (forming associates) is shifted to higher wavelength (lower energy) as compared to Ce^{3+} coordinated with only regular O^{2-} ions, because O_{Me} is more covalently bonded to Ce^{3+} as compared to the regular O^{2-} ions, resulting in larger redshift of the 5d center of gravity (nephelauxetic effect).

To be clearer, the structure chart is performed to explain the origin of luminescence, as shown in Figure 4a-4b. So in $\text{CeAl}_{11}\text{O}_{18}$ crystal lattice, there are two types of luminescent Ce^{3+} sites imposed by different crystal field. It can be proved by the excitation spectra, which covers two bands at 260 nm and 320 nm as the monitored emission peak is 450 nm. A main excitation peak at 260 nm is observed as the monitored emission peak is 350 nm. Under 320 nm excitation, $\text{CeAl}_{11}\text{O}_{18}$ only gives blue emission.

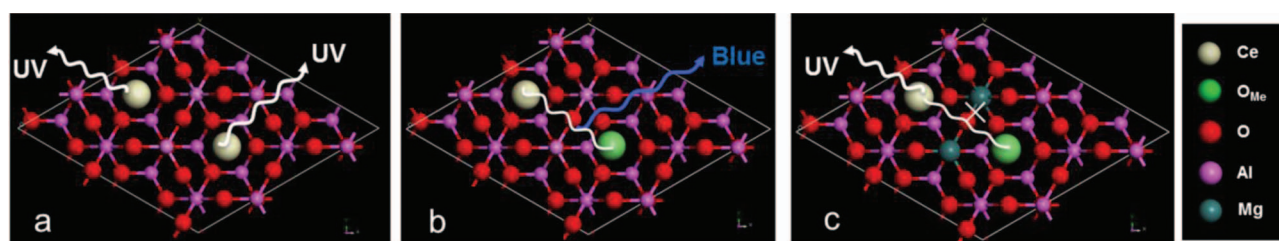


Figure 4. Representation of the luminescence mechanism projected along [001] direction. a. $\text{CeAl}_{11}\text{O}_{18}$ structure gives UV emission, which is ascribed to 5d-4f electron transition of normal Ce^{3+} ; b. blue emission of $\text{CeAl}_{11}\text{O}_{18}$ phosphor is ascribed to Ce- O_{Me} associates; c. Mg ions remove the Ce- O_{Me} associate, resulting in UV emission only.

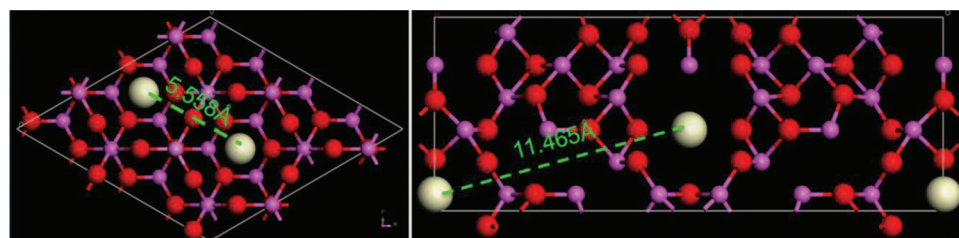


Figure 5. Representation of Ce-Ce distance projected along [001] and [110] direction respectively in $\text{CeAl}_{11}\text{O}_{18}$ crystal lattice.

These results indicate that 260 nm should be responsible for the UV emission band ascribed to normal Ce^{3+} while 320 nm should be responsible for the blue emission band ascribed to Ce- O_{Me} associates. The most noteworthy is that energy transfer from normal Ce^{3+} to Ce- O_{Me} associates is very effective because the blue emission becomes the predominant band for $\text{CeAl}_{11}\text{O}_{18}$ phosphor under 260 nm excitation.

If Mg^{2+} is doped into $\text{CeAl}_{11}\text{O}_{18}$ lattice, the interaction between Ce^{3+} and O_{Me} seems to be screened (i.e. no Ce- O_{Me} associates present anymore), resulting in absence of blue emission in the final phosphor, (Figure 4c). So $\text{CeMgAl}_{11}\text{O}_{19}$ as shown in Figure 3, just gives only UV emission. Due to the magnetoplumbite-structure with ideal stoichiometry (large-cation/small-cation/anion = 1/12/19), no O_{Me} ions are expected to be present in $\text{CeMgAl}_{11}\text{O}_{19}$ like in $\text{CeAl}_{12}\text{O}_{18}\text{N}$. As a result, no blue emission due to 5d-4f transitions of Ce^{3+} coordinated with O_{Me} can be observed (Fig. 3). So Mg doping will play an important role in disappearance of O_{Me} (in agreement with a previous report),¹¹ and a similar effect can be realized with N doping.

According to previous research on Ce doped phosphors, the general critical distance corresponding to concentration quenching of luminescent ions in the matrix is almost more than 7 Å.²⁵⁻³⁰ It means that the interaction between luminescent ions is strong at this inter-ionic distance. In the $\text{CeAl}_{11}\text{O}_{18}$ crystal lattice, there is only one type of Ce site and the neighbored Ce-Ce distance is different. The nearest Ce-Ce distance is 5.558 Å in [001] plane, whereas for the [110] plane, the Ce-Ce distance is up to 11.465 Å, as shown in Figure 5. But it is easily concluded that Ce- O_{Me} associates with short distance show stronger interaction than that with long distance. So it is reasonable to discuss the case in the [001] plane instead of [110] plane in the $\text{CeAl}_{11}\text{O}_{18}$ crystal lattice, just like what has been discussed above in Figure 4.

$\text{CeAl}_{11(1-x)}\text{Si}_{11x}\text{O}_{18-11x}\text{N}_{11x}$.— Many aluminates based phosphors have been researched to improve their luminescence properties by doping Si-N.³¹⁻⁴⁰ Like BAM: Eu^{2+} blue-emitting phosphor, aluminates phosphors suffer from serious deterioration of luminescence efficiency during continuous excitation in fluorescent lamps.⁴¹ Wang et al. have successfully proposed a new method of Si-N doping in BAM: Eu^{2+} phosphor to improve its luminescence intensity and thermal stability.³² In this part, the structure and luminescence properties are also studied in terms of effects of Si-N doping.

Figure 6 shows the XRD patterns of synthesized powders with the composition of $\text{CeAl}_{11(1-x)}\text{Si}_{11x}\text{O}_{18-11x}\text{N}_{11x}$. A single phase with magnetoplumbite structure is still formed when the doping concentration

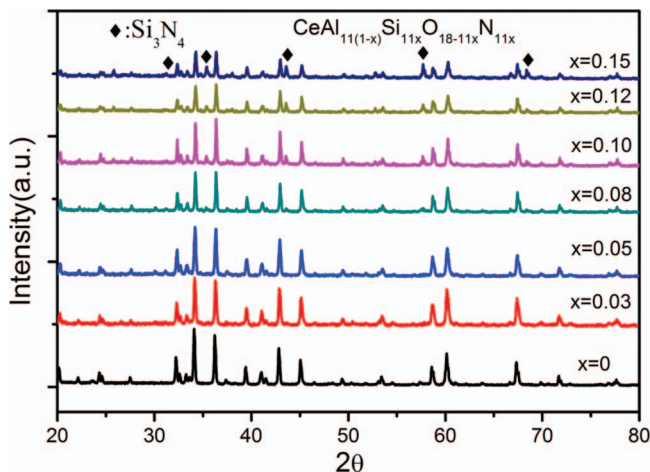


Figure 6. XRD patterns of $\text{CeAl}_{11(1-x)}\text{Si}_{11x}\text{O}_{18-11x}\text{N}_{11x}$. x ranges from 0 to 0.15.

of Si-N is less than 0.08. The impurity of Si_3N_4 gradually appears with further increase of the content of the starting material Si_3N_4 , indicating that the solubility limit of Si-N doped into $\text{CeAl}_{11}\text{O}_{18}$ crystal lattice is approximately 0.08 by solid state reaction. Meanwhile, with the more Si-N doping in powders, the crystallinity of $\text{CeAl}_{11}\text{O}_{18}$ turns worse. The reason is the substitution of Si-N will bring in defects, which destroys the periodic structure of $\text{CeAl}_{11}\text{O}_{18}$ crystal lattice.

The energy-dispersive X-ray spectroscopy (EDS) is introduced to analyze the $\text{CeAl}_{11}\text{O}_{18}$ and $\text{CeAl}_{11(1-x)}\text{Si}_{11x}\text{O}_{18-11x}\text{N}_{11x}$ ($x = 0.08$) chemical compositions qualitatively. Figure 7 shows the EDS spectra of the samples, in which elements of Ce, Al, O and Ce, Al, O, Si, N are examined respectively, indicating that the Si-N is present in the host lattice of the $\text{CeAl}_{11(1-x)}\text{Si}_{11x}\text{O}_{18-11x}\text{N}_{11x}$ structure.

The dissolution of Si-N in $\text{CeAl}_{11}\text{O}_{18}$ lattice could also be proved by the decrease of crystal lattice parameters with increasing Si_3N_4 content. As shown in the inset of Figure 8, with increasing Si_3N_4 content, the major $\text{CeAl}_{11}\text{O}_{18}$ diffraction peaks at $\sim 34.2^\circ$ and 36.3° shifts to a higher angle. It is clearly seen that the hexagonal lattice parameters of $\text{CeAl}_{11}\text{O}_{18}$ are decreased for higher doped Si_3N_4 contents in terms of calculated results by Unit Cell software based on XRD peaks. This crystal lattice reduction is likely due to the shorter bond length for Si-N bond (168.5–176 pm in Si_3N_4) versus Al-O bond (176.1 pm). When the dopant concentration of Si-N is more than 0.1, the crystal lattice parameters almost remain constant, indicating that the amount of Si-N doped into $\text{CeAl}_{11}\text{O}_{18}$ lattice has been saturated. The ratio of the lattice parameters (c/a) nicely fits the dependence of the various alkaline-earth hexaaluminates with a (disordered) magnetoplumbite or β -alumina-type structure.¹² For Si-N doped $\text{CeAl}_{11}\text{O}_{18}$ powders, the c/a ratio is nearly constant and its value is always below 3.96,

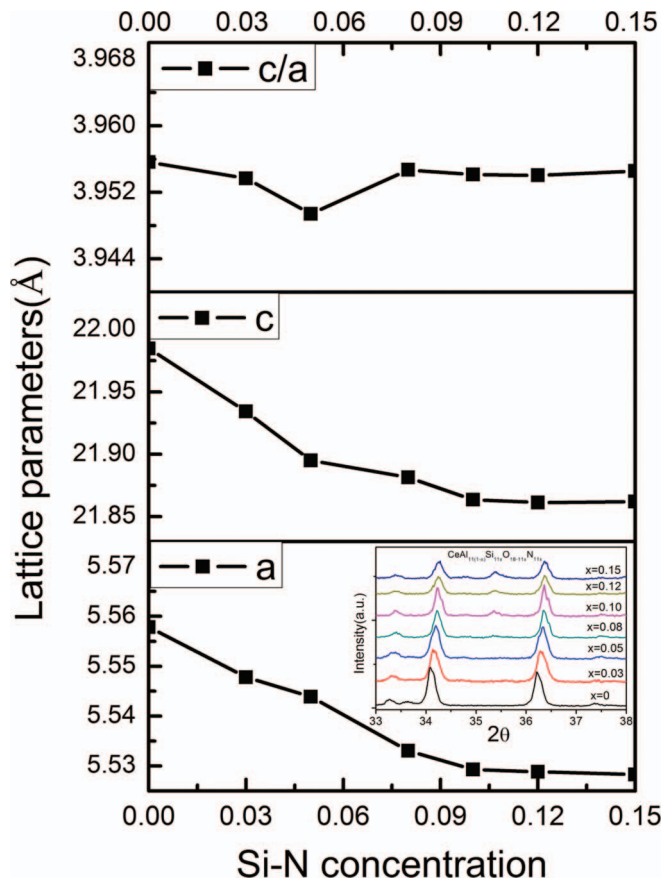


Figure 8. Lattice parameters of $\text{CeAl}_{11(1-x)}\text{Si}_{11x}\text{O}_{18-11x}\text{N}_{11x}$ as a function of x .

indicating that the structure of Si-N doped $\text{CeAl}_{11}\text{O}_{18}$ powders remains disordered magnetoplumbite-type structure similar to undoped $\text{CeAl}_{11}\text{O}_{18}$.

Figure 9 shows the luminescence properties of Si-N doped $\text{CeAl}_{11}\text{O}_{18}$ phosphors. It is clearly seen that the emission peak of the phosphors gradually changes from blue to UV by Si-N doping excited by UV light of 260 nm. More Si-N doping results in larger percentage of UV emission in the whole emission spectrum. Blue emission ascribed to Ce-O_{Mc} associates seems to be effectively screened. For example, when the Si-N concentration reaches 0.08 in $\text{CeAl}_{11(1-x)}\text{Si}_{11x}\text{O}_{18-11x}\text{N}_{11x}$ system, the UV emission becomes dominant absolutely. The excitation spectra are also shown in Figure 9. It is clearly seen that the intensity of the excitation peak at 320 nm gradually decreases and the excitation peak at 260 nm becomes dominant. According to the analysis of the luminescence properties of

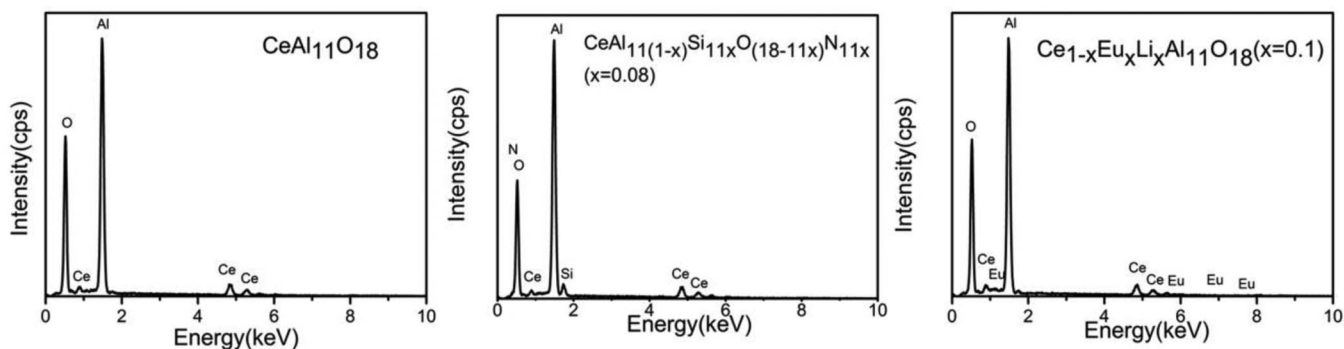


Figure 7. EDS images of $\text{CeAl}_{11}\text{O}_{18}$, $\text{CeAl}_{11(1-x)}\text{Si}_{11x}\text{O}_{18-11x}\text{N}_{11x}$ ($x = 0.08$) and $\text{Ce}_{1-x}\text{Eu}_x\text{LiAl}_{11}\text{O}_{18}$ ($x = 0.1$).

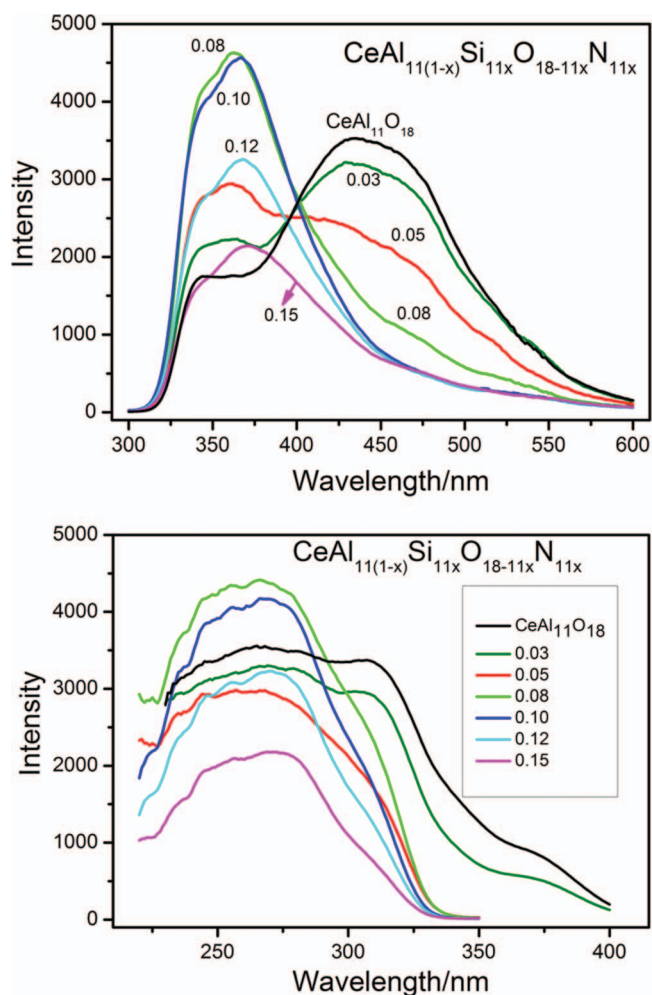


Figure 9. Excitation and emission spectra of the powders with composition of $\text{CeAl}_{11(1-x)}\text{Si}_{11x}\text{O}_{18-11x}\text{N}_{11x}$. The excitation wavelength is 260 nm for emission spectra. The monitored emission wavelength is the highest emission peak for excitation spectra.

$\text{CeAl}_{11}\text{O}_{18}$ and $\text{CeMgAl}_{11}\text{O}_{19}$, it is concluded that Si-N doping results in a decrease of O_{Me} ions in $\text{CeAl}_{11}\text{O}_{18}$. Driving force could be the formation of a compound with ideal magnetoplumbite-stoichiometry, like $\text{CeAl}_{12}\text{O}_{18}\text{N}$. The compound $\text{CeAl}_{12}\text{O}_{18}\text{N}$ can be deduced from $\text{SrAl}_{12}\text{O}_{19}$ with ideal magnetoplumbite-stoichiometry by replacing (SrO) by (CeN).¹³ To figure out this question, therefore, $\text{CeAl}_{12}\text{O}_{18}\text{N}$ is produced and its spectra are described before in this paper. As seen in Figure 3, $\text{CeAl}_{12}\text{O}_{18}\text{N}$ shows a single UV emission similar to $\text{CeMgAl}_{11}\text{O}_{19}$. So the synthesized powders with composition of $\text{CeAl}_{11(1-x)}\text{Si}_{11x}\text{O}_{18-11x}\text{N}_{11x}$ tend to form $\text{CeAl}_{12}\text{O}_{18}\text{N}$ phase instead of a compound $\text{CeAl}_{11}\text{O}_{18}$ phase. Unfortunately, both structures can't be easily discriminated due to uniform XRD date. In all cases, superimposed broad bands are observed. For Ce^{3+} ions with D3h local symmetry in $\text{CeAl}_{11}\text{O}_{18}$ crystal lattice, it is expected that the excited 5d energy levels of Ce^{3+} are split into three sublevels. Indeed, three excitation bands can be distinguished in the spectra (see Fig. 9). The 5d energy level of Ce^{3+} is very sensitive to the local environment, as well as Eu^{2+} .⁴² So some difference in excitation spectra is observed due to crystal field change before and after Si-N is doped into $\text{CeAl}_{11}\text{O}_{18}$ crystal lattice.

It is generally reported that the emission occurs at longer wavelength with more nitrogen doping attributable to the decrease of crystal lattice parameters and the lower electronegativity of nitrogen (3.04) compared with oxygen (3.44) (i.e. nephelauxetic effect), which results in stronger crystal-field splitting and lower energy of the center

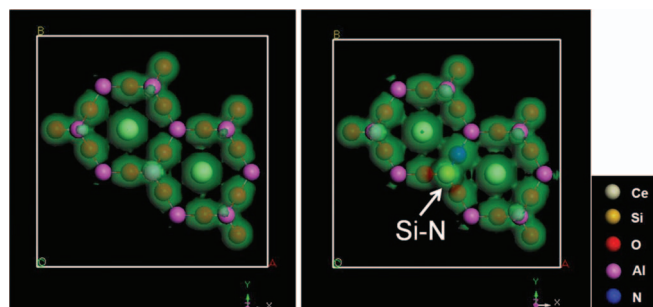


Figure 10. Comparison of calculated electron clouds of $\text{CeAl}_{11}\text{O}_{18}$ and $\text{CeAl}_{11(1-x)}\text{Si}_{11x}\text{O}_{18-11x}\text{N}_{11x}$ projected along [001] plane.

of gravity of the 5d levels of Ce^{3+} .⁴³⁻⁴⁵ But here, an absolutely opposite result is exhibited. The emission changes from blue to UV with Si-N doping. Why this phenomenon happens is that the luminescence mechanism is different basically. For $\text{CeAl}_{11}\text{O}_{18}$ phosphor, its UV and blue luminescence originates from two parts: normal Ce^{3+} ions and Ce-O_{Me} associates respectively. Si-N doping leads to the disappearance of O_{Me} ions. So it is observed that blue emission gradually decreases and UV emission becomes stronger with the increase of Si-N doping in $\text{CeAl}_{11}\text{O}_{18}$ crystal lattice.

In order to further clarify the influence of Si-N doping on luminescence, Ce clusters $[\text{Ce}_2\text{Al}_{15}\text{O}_{15}]^{21+}$ and $[\text{Ce}_2\text{Al}_{14}\text{SiO}_{14}\text{N}]^{21+}$ are constructed and first-principles calculations of electron clouds are performed. Figure 10 shows the calculated electron clouds of $\text{CeAl}_{11}\text{O}_{18}$ and Si-N doped $\text{CeAl}_{11}\text{O}_{18}$. It is assumed that Si-N pairs are located around Ce^{3+} in the mirror plane, which will be discussed later. An expanded electron cloud is intuitively shown due to higher formal charge of N^{3-} compared with O^{2-} and more covalent nature of the metal-nitrogen chemical bonding versus metal-oxygen.²⁵ Si-N doping should play a role in shifting the UV luminescence spectra of normal Ce^{3+} ions to longer wavelength theoretically. As seen in Figure 9, a small redshift of UV emission peak is truly observed due to stronger crystal-field splitting of the 5d levels of Ce^{3+} and nephelauxetic effect caused by Si-N doping.

Based on the above analysis, the UV emission is ascribed to normal Ce^{3+} in $\text{CeAl}_{11}\text{O}_{18}$ crystal lattice and blue emission is ascribed to Ce-O_{Me} associates. It is concluded that due to Si-N incorporation the O_{Me} disappears gradually and Ce-O_{Me} associates collapse and turn to normal Ce^{3+} ions, resulting in UV emission again in Si-N doped $\text{CeAl}_{11}\text{O}_{18}$. Hence, the total quantity of effective luminescent centers is fixed although Si-N doping changes the proportion of Ce^{3+} and Ce-O_{Me} associates. Figure 11 exhibits the sum of luminescence intensity of UV emission peak at 350 nm and blue emission peak at 450 nm. With the Si-N doping concentration below 10%, the sum is almost balanced, indicating the result sounds logical that two kinds of luminescence centers (normal Ce^{3+} ions and Ce-O_{Me} associates) can be conversed by Si-N doping. In a previous study, it has been pointed out that the number of O_{Me} is $\sim 14\%$ in single $\text{CeAl}_{11}\text{O}_{18}$,¹¹ which is coincident with the critical concentration of 10% of Si-N

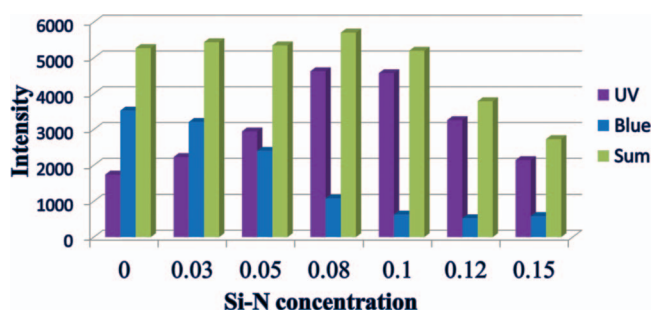


Figure 11. Sum of luminescence intensity of UV emission band and blue emission band as a function of x in $\text{CeAl}_{11(1-x)}\text{Si}_{11x}\text{O}_{18-11x}\text{N}_{11x}$.

donant from the view of order of magnitude. It seems that one Si-N doping corresponds to disappearance of one Ce- O_{Me} associate. It has been researched carefully about Si-N location in Si-N doped $BaMgAl_{10}O_{17}:Eu^{2+}$ phosphor using CASTEP code, which can give us a significant reference because of the almost similar hexagonal crystal structure between $BaMgAl_{10}O_{17}$ and $CeAl_{11}O_{18}$.⁴⁶ The results show the total systematic energy is the lowest among dozens of structural model when Si and N atoms are connected to each other and one Si-N bond replaces one Al-O bond around rare-earth in mirror plane in $BaMgAl_{10}O_{17}:Eu^{2+}$ crystal lattice, which well agreed with the EPR, XAFS and TL experimental results. For Si-N doped $CaAl_2O_4$ phosphor, it is also found that Si-N bonds prefer to replace Al-O bonds around Eu^{2+} ions by the analysis of electron paramagnetic resonance (EPR) spectra.³⁴ So it can be concluded and also expected from local charge balance considerations that one connected Si-N bond is substituted for one Al-O bond around Ce^{3+} in the mirror plane of $CeAl_{11}O_{18}$. This conclusion can better explain the corresponding relationship between doped Si-N concentration ($\sim 10\%$) and the number of O_{Me} ($\sim 14\%$). But so far, it is still unknown about the exact mechanism how Si-N doping decreases O_{Me} ions. It is possibly related to the fact that N^{3-} cannot well stabilize O^{2-} ions because of larger nephelauxetic effect of N^{3-} . The coexistence of N^{3-} and O_{Me} will bring in higher energy of the system, resulting in unstable structure of $CeAl_{11}O_{18}$ crystal lattice. This analysis needs more detailed calculation.

From Figures 9 and 11, it is observed that the luminescence intensity of Si-N doped $CeAl_{11}O_{18}$ phosphors decreases when Si-N doping concentration is more than 10%. In order to explain such behavior, defects caused by doping Si-N into $CeAl_{11}O_{18}$ host should be considered.⁴⁷ More Si-N dissolution brings defects into $CeAl_{11}O_{18}$ crystal lattice, leading to lattice distortion and lattice imperfection due to the shorter bond length for Si-N bond compared with Al-O bond and due to deviations from ideal magnetoplumbite stoichiometry. FTIR can tell us more about the inner structural change of Si-N doped $CeAl_{11}O_{18}$ phosphors. As shown in Figure 12, $CeAl_{11}O_{18}$ phosphors show infrared absorption ranging mainly from 900 to 450 cm^{-1} , which are ascribed to AlO_4 and AlO_6 vibrations.⁴⁸ The appearance of infrared Si-N and Si-O vibrations in $CeAl_{11}O_{18}$ lattice with increasing the Si-N doping, also indicates the successful dissolution of connected Si-N bond. The FTIR data show that the absorption band of AlO_4 and AlO_6 becomes broader, the intensity becomes smaller due to defects induced by increasing Si-N doping while unreacted Si_3N_4 phase is detected in the product when the doping concentration of Si-N is more than 10%, which is in agreement with XRD results of Figure 6. So the luminescence decrease is due to defects caused by Si-N doping and residual Si_3N_4 impurity.

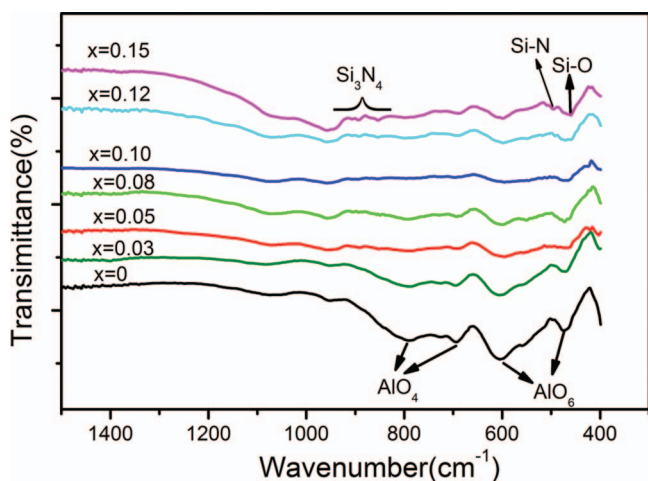


Figure 12. FTIR spectra as a function of x in $CeAl_{11(1-x)}Si_{11x}O_{18-11x}N_{11x}$.

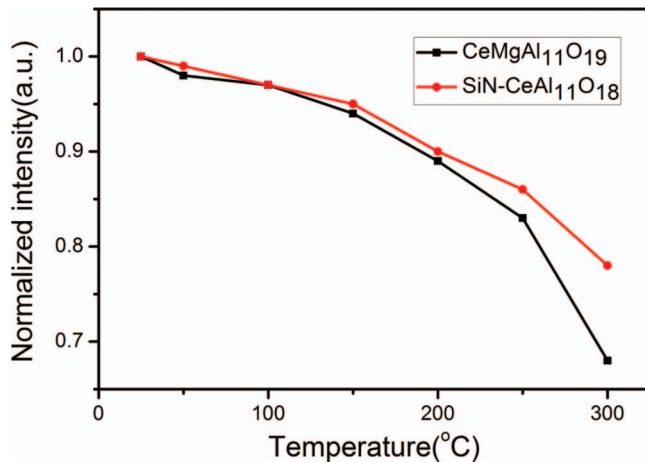


Figure 13. Temperature dependence of emission intensity for $CeAl_{11}O_{18}$ and $CeAl_{11(1-x)}Si_{11x}O_{(18-11x)}N_{(11x)}$ ($x = 0.1$).

In high-power lighting and display devices, the parameter of high quenching temperature is very crucial to maintain their smooth operation. Figure 13 is the influence of temperature on the intensity of the emission peak of $CeMgAl_{11}O_{19}$ and $CeAl_{11(1-x)}Si_{11x}O_{18-11x}N_{11x}$ phosphors ($x = 0.1$). In both cases, the emission intensities decrease with increasing temperature, but Si-N incorporation minimizes the temperature effect on thermal quenching, compared with $CeMgAl_{11}O_{19}$ phosphor. For example, The emission intensity of the Si-N doped $CeAl_{11}O_{18}$ phosphor at 250°C remains at 86% of the intensity measured at room temperature, whereas only 83% for $CeMgAl_{11}O_{19}$ phosphor.¹⁵

Thermal quenching is related to thermal ionization of the 5d electron to the conduction band states or energy level crossing between the lowest energy 5d level and the 4f ground states.^{25,46,49} A strong $N^{3-}-Ce^{3+}$ covalent bond is expected to suppress the electronic transition from the 5d levels to the bottom of the conduction band. Moreover Si-N incorporation leads to the increasing stiffness of the crystal structure and lattice shrinkage because the shorter bond length of Si-N versus Al-O bond, resulting in uneasy nonradiative relaxation of Ce^{3+} . Both factors should contribute to smaller thermal quenching after the Si-N incorporation.

$Ce_{1-x}Eu_xLi_xAl_{11}O_{18}$.— Ce doped phosphors often yield short wavelength emission and Eu doped phosphors yield long wavelength emission in the same matrix. Hence, it is possible for energy transfer from Ce^{3+} to Eu^{2+} if the emission spectrum of Ce^{3+} and the excitation spectrum of Eu^{2+} are significantly overlapping, which has been reported in many $Ce^{3+}-Eu^{2+}$ codoped hosts.⁵⁰⁻⁵⁵ For $CeAl_{11}O_{18}$ phosphor, it yields UV and blue emission when excited by 260 nm. In Eu doped hexaaluminates, most of them have strong absorption in UV band from 250 to 400 nm. For example, $EuMgAl_{10}O_{17}$ shows absorption band from 300 to 400 nm and yields blue emission,⁵⁶ as seen in Figure 14. Another example is the famous commercial phosphor BAM: Eu^{2+} , which can effectively convert UV band from 250 to 400 nm into blue emission.³² The effective resonant energy transfer is expected based on the significant spectral overlap between the UV part of the emission spectrum of Ce^{3+} and the excitation spectrum of Eu^{2+} and consequently a single blue-emitting phosphor can be obtained.

The phase identification for the synthesized powders with the composition of $Ce_{1-x}Eu_xLi_xAl_{11}O_{18}$ is researched by XRD, as seen in Figure 15. All diffraction peaks of the Eu, Li codoped samples are consistent with those of $CeAl_{11}O_{18}$ when x ranges from 0 to 0.1, indicating Eu, Li ions are completely dissolved into the $CeAl_{11}O_{18}$ crystal lattice. EDS result also verifies this conclusion, as shown in Figure 7, in which elements of Ce, Al, O and Eu are examined. Not like Si-N doped $CeAl_{11}O_{18}$, Eu-Li codoping does not lead to the change of lattice parameters, as shown in Figure 16. Eu^{2+} ions occupy Ce^{3+}

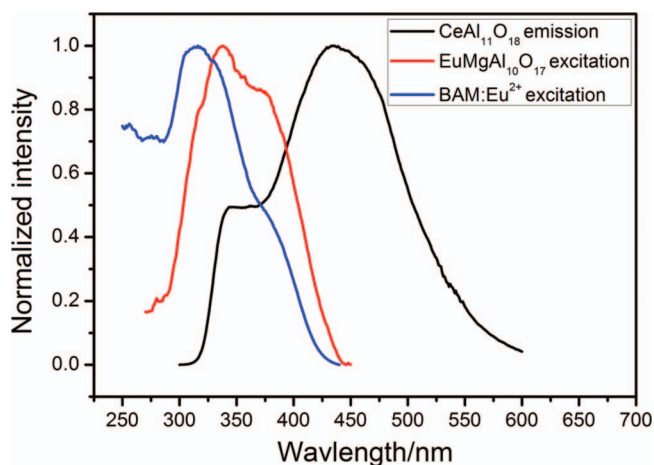


Figure 14. Emission spectrum of $\text{CeAl}_{11}\text{O}_{18}$ and excitation spectra of $\text{EuMgAl}_{10}\text{O}_{17}$ and BAM:Eu^{2+} .

sites, accompanied by the charge balance by Li^+ ions. Because of the small radius of Li^+ (90 pm, CN = 6),⁵⁷ Li^+ can enter the interstitial sites of $\text{CeAl}_{11}\text{O}_{18}$ crystal lattice.⁵⁸ The crystal structure of $\text{CeAl}_{11}\text{O}_{18}$ shows there is large space at the location of Ce^{3+} sites in the mirror plane as seen in Figure 1. It reveals some degree of tolerance for Eu-Li codoping, although Eu^{2+} (131 pm, CN = 6) has larger radius than Ce^{3+} ions (115 pm, CN = 6) compensated by Li^+ codoping. So the crystal structure and lattice parameters are kept stable after Eu-Li codoping.

Figure 17 shows the excitation and emission spectra of the powders with composition of $\text{Ce}_{1-x}\text{Eu}_x\text{Li}_x\text{Al}_{11}\text{O}_{18}$ with different dopant contents x . Under excitation at 260 nm, the emission intensity of UV band is found to decrease, whereas the intensity of the blue band increases with increasing Eu-Li doping content. The UV emission finally disappears and blue emission reaches a maximum at $x = 0.03$, and then decreases with further increasing Eu-Li doping content, which is mainly attributed to energy reabsorption among the nearest Eu^{2+} or Ce^{3+} ions. From the emission spectrum of 3% Eu-Li doping, the CIE chromaticity coordinate is determined to be (0.162, 0.172), corresponding to a blue emission. The excitation spectra show no obvious change in shape between $\text{CeAl}_{11}\text{O}_{18}$ and Eu-Li codoped $\text{CeAl}_{11}\text{O}_{18}$ phosphors. The observed variations in the emission intensities and unchanged shape in excitation spectra of $\text{Ce}_{1-x}\text{Eu}_x\text{Li}_x\text{Al}_{11}\text{O}_{18}$ phosphors strongly indicate the energy transfer from the Ce^{3+} to Eu^{2+} . So the total observed blue emission should come from two parts: 1. Ce-O_{Mc}

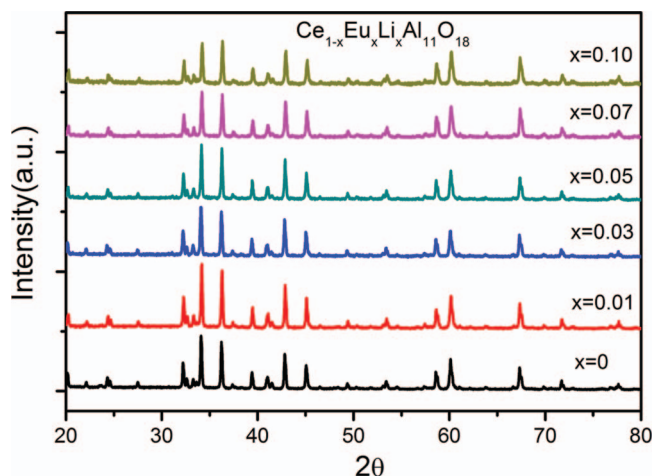


Figure 15. XRD patterns of $\text{Ce}_{1-x}\text{Eu}_x\text{Li}_x\text{Al}_{11}\text{O}_{18}$. x ranges from 0 to 0.10.

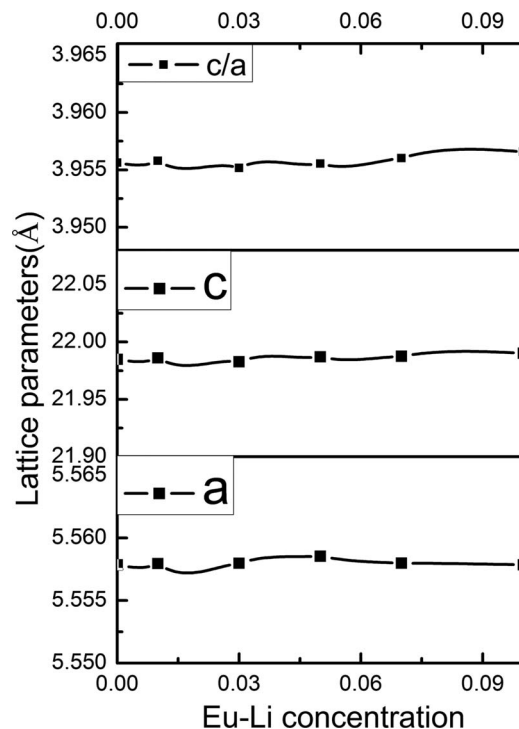


Figure 16. Lattice parameters with the increase of Eu-Li doping.

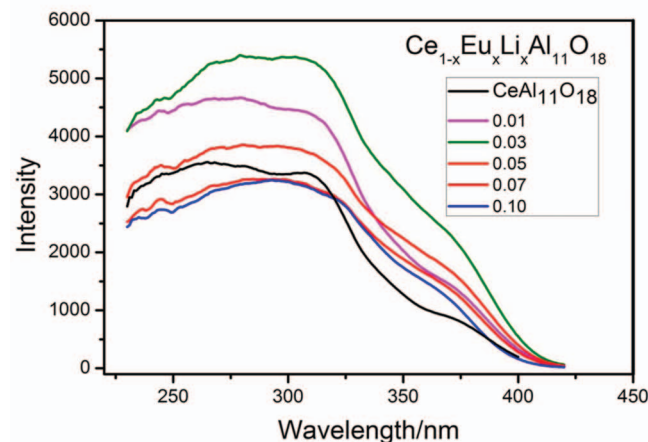
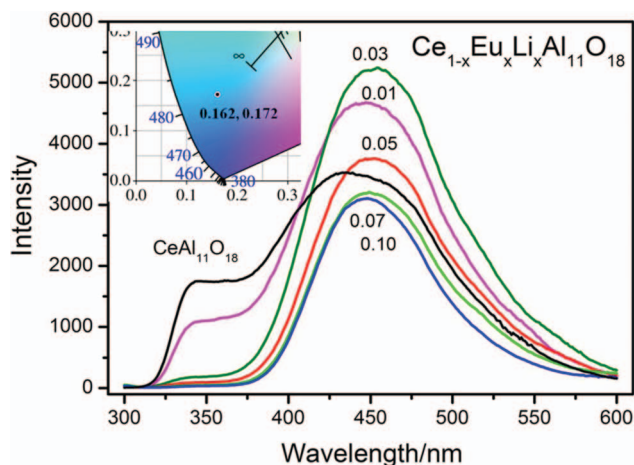


Figure 17. Excitation and emission spectra of the powders with composition of $\text{Ce}_{1-x}\text{Eu}_x\text{Li}_x\text{Al}_{11}\text{O}_{18}$. The excitation wavelength is 260 nm for emission spectra. The monitored emission wavelength is 450 nm for excitation spectra.

associates discussed before. $2.4f^{65d^1} \rightarrow 4f^7$ transition of Eu^{2+} ions, which are overlapping together.

To explain the strong blue emission intensity intuitively, Eu-Li codoped phosphor ($x = 0.03$) is used to compare with commercial BAM: Eu^{2+} phosphor (Guangzhou Research Institute of Nonferrous Metals, China). The absolute emission intensity of Eu-Li codoped phosphor ($x = 0.03$) reaches 60% relative to that of well-known BAM: Eu^{2+} phosphor. It is worth mentioning that the quantum efficiency of 3% Eu-Li codoped phosphor could be further increased by doping other metal ions and optimization of its crystallinity and morphology, making it a promising blue-emitting phosphor for use in display equipments.

Conclusions

The synthesis, structure and luminescence properties of Si-N or Eu-Li codoped $\text{CeAl}_{11}\text{O}_{18}$ phosphors are investigated carefully.

For Si-N doped $\text{CeAl}_{11}\text{O}_{18}$, Si-N doping can be successfully dissolved into $\text{CeAl}_{11}\text{O}_{18}$, which is proved by the shrinkage of crystal lattice due to the shorter bond length for Si-N bond versus Al-O bond. Because Si-N doping leads to the disappearance of O_{Me} ions, blue Ce^{3+} emission gradually decreases and UV Ce^{3+} emission becomes stronger with the increase of Si-N doping in $\text{CeAl}_{11}\text{O}_{18}$ crystal lattice. Compared with the traditional UV-emitting phosphor $\text{CeMgAl}_{11}\text{O}_{19}$, Si-N doped $\text{CeAl}_{11}\text{O}_{18}$ shows less thermal quenching.

For Eu-Li doped $\text{CeAl}_{11}\text{O}_{18}$, a single blue-emitting phosphor can be obtained by Eu-Li codoping because of the energy transfer from Ce^{3+} (UV emission) to Eu^{2+} . The emission intensity of Eu-Li codoped phosphor ($x = 0.03$) reaches 60% of commercial BAM: Eu^{2+} phosphor, making it a potential candidate in display devices after optimization of its luminescence properties.

Acknowledgment

This research was supported by the National Natural Science Foundation of China (Grant No. 51302029), National Thousand Talent Project and the Fundamental Research Funds for the Central Universities (Grant No. A03010023801115).

References

- I. Y. Jung, Y. Cho, S. G. Lee, S. H. Sohn, D. K. Kim, D. K. Lee, and Y. M. Kweon, *Appl. Phys. Lett.*, **87**, 19 (2005).
- V. Singh, T. K. G. Rao, and J. J. Zhu, *J. Lumin.*, **126**, 1 (2007).
- T. Murata, T. Tanoue, M. Iwasaki, K. Morinaga, and T. Hase, *J. Lumin.*, **114**, 207 (2005).
- S. D. Ahn, H. S. Jeong, D. C. Choo, T. W. Kim, J. Y. Lee, J. H. Park, and M. S. Kwon, *J. Nanosci. Nanotechnol.*, **11**, 1770 (2011).
- J. M. P. J. Versteegen, J. L. Sommerdijk, and J. G. Verriet, *J. Lumin.*, **6**, 425 (1973).
- J. L. Sommerdijk, van der Does de Bye, and J. A. W. P. H. J. M. Verberne, *J. Lumin.*, **14**, 91 (1976).
- S. R. Jansen, J. M. Migchels, H. T. Hintzen, and R. Metselaar, *J. Electrochem. Soc.*, **146**, 800 (1999).
- R. J. Xie and H. T. Hintzen, *J. Am. Ceram. Soc.*, **96**, 665 (2013).
- L. J. Yin, Q. Q. Zhu, W. Yu, L. Y. Hao, X. Xu, F. C. Hu, and M. H. Lee, *J. Appl. Phys.*, **111**, 053534 (2012).
- L. J. Yin, X. Xu, W. Yu, J. G. Yang, L. X. Yang, X. F. Yang, L. Y. Hao, and X. J. Liu, *J. Am. Ceram. Soc.*, **93**, 1702 (2010).
- A. L. N. Stevels, *J. Electrochem. Soc.*, **125**, 588 (1978).
- H. T. Hintzen, R. Hanssen, S. R. Jansen, and R. Metselaar, *J. Solid State Chem.*, **142**, 48 (1999).
- S. R. Jansen, J. W. de Haan, L. J. M. van de Ven, R. Hanssen, H. T. Hintzen, and R. Metselaar, *Chem. Mater.*, **9**, 1516 (1997).
- R. W. Wolfe, Ultraviolet emitting Ce alkaline earth aluminate lamp phosphors and lamps utilizing same. U. S. Patent 4,246,630, Jan. 20 (1981).
- R. W. Wolfe, Cerium magnesium aluminate luminescent compositions, and lamps utilizing same. U. S. Patent 4,088,922, May 9 (1978).
- P. W. Ranby and D. Y. Hobbs, Method of preparing cerium and terbium activated aluminate phosphors. U. S. Patent 4,096,088, Jun. 20 (1978).
- R. W. Wolfe, Ultraviolet emitting CeYmg aluminate fluorescent lamp phosphor for psoriasis treatment. U. S. Patent 4,153,572, May 8 (1979).
- Y. C. Cheng, X. L. Wu, J. Zhu, L. L. Xu, S. H. Li, and P. K. J. Chu, *Appl. Phys.*, **103**, 073707 (2008).
- M. D. Segall, P. J. D. Lindan, M. J. Probert, C. J. Pickard, P. J. Hasnip, S. J. Clark, and M. C. Payne, *J. Phys.: Condens. Matter*, **14**, 2717 (2002).
- C. J. Duan, X. J. Wang, and J. T. Zhao, *J. Appl. Phys.*, **101**, 023501 (2007).
- J. P. Perdew, K. Burke, and M. Ernzerhof, *Phys. Rev. Lett.*, **77**, 3865 (1996).
- D. M. Ceperley and B. Alder, *J. Phys. Rev. Lett.*, **45**, 566 (1980).
- J. P. Perdew and A. Zunger, *Phys. Rev. B*, **23**, 5048 (1981).
- M. Gasperin, M. C. Saine, A. Kahn, F. Laville, and A. M. Lejus, *J. Solid State Chem.*, **54**, 61 (1984).
- A. A. Setlur, W. J. Heward, M. E. Hannah, and U. Happek, *Chem. Mater.*, **20**, 6277 (2008).
- Z. G. Xia and R. S. Liu, *J. Phys. Chem. C*, **116**, 15604 (2012).
- J. H. Kim and K. Y. Jung, *J. Lumin.*, **131**, 1487 (2011).
- Y. F. Wang, X. Xu, H. Qin, L. J. Yin, and L. Y. Hao, *J. Rare Earths*, **28**, 281 (2010).
- N. Guo, *J. Phys. Chem. C*, **114**, 18051 (2010).
- Y. C. Fang, X. R. Huang, H. Y. Lin, and S. Y. Chu, *J. Am. Ceram. Soc.*, **94**, 2735 (2011).
- H. H. Lin, G. B. Zhang, P. A. Tanner, and H. B. Liang, *J. Phys. Chem. C*, **117**, 12769 (2013).
- Y. F. Wang, X. Xu, L. J. Yin, and L. Y. Hao, *Electrochem. Solid-State Lett.*, **13**, J119 (2010).
- Y. F. Wang, X. Xu, L. J. Yin, and L. Y. Hao, *J. Am. Ceram. Soc.*, **93**, 1534 (2010).
- Y. F. Wang, X. Xu, H. Qin, L. J. Yin, and L. Y. Hao, *J. Rare Earths*, **28**, 281 (2010).
- Q. Q. Zhu, L. X. Yang, W. W. Ji, and X. Xu, *J. Chin. Rare Earth Soc.*, **31**, 44 (2013).
- M. Sopicca-Lizer, D. Michalik, J. Plewa, T. Juestel, H. Winkler, and T. Pawlik, *J. Eur. Ceram. Soc.*, **32**, 1383 (2012).
- B. T. Liu, B. Y. Han, F. Zhang, Y. Wen, G. Zhu, J. Zhang, and Y. H. Wang, *Mater. Res. Bull.*, **47**, 156 (2012).
- G. Anoop, I. H. Cho, D. W. Suh, C. K. Kim, and J. S. Yoo, *J. Lumin.*, **134**, 390 (2013).
- Y. C. Fang, P. C. Kao, and S. Y. Chu, *J. Electrochem. Soc.*, **158**, J120 (2011).
- Y. Q. Li, N. Hirosaki, R. J. Xie, and M. Mitomo, *Sci. Technol. Adv. Mat.*, **8**, 607 (2007).
- A. A. Setlur, W. J. Heward, M. E. Hannah, and U. Happek, *Chem. Mater.*, **20**, 6277 (2008).
- K. B. Kim, K. W. Koo, T. Y. Cho, and H. G. Chun, *Mater. Chem. Phys.*, **80**, 682 (2003).
- K. Takahashi, N. Hirosaki, R. J. Xie, M. Harada, K. I. Yoshimura, and Y. Tomomura, *Appl. Phys. Lett.*, **91**, 091923 (2007).
- J. W. H. van Krevel, H. T. Hintzen, R. Metselaar, and A. Meijerink, *J. Alloys Compd.*, **268**, 272 (1998).
- R. J. Xie, N. Hirosaki, M. Mitomo, K. Sakuma, and N. Kimura, *Appl. Phys. Lett.*, **89**, 241103 (2006).
- Y. Q. Li, N. Hirosaki, R. J. Xie, J. Li, T. Takeda, Y. Yamamoto, and M. Mitomo, *J. Am. Ceram. Soc.*, **92**, 2738 (2009).
- Y. F. Wang, Y. F. Wang, Q. Q. Zhu, L. Y. Hao, X. Xu, R. J. Xie, and S. Agathopoulos, *J. Am. Ceram. Soc.*, **96**, 2562 (2013).
- M. Bosca, L. Pop, G. Borodi, P. Pascuta, and E. Culea, *J. Alloys Compd.*, **479**, 579 (2009).
- N. R. Yang and W. H. Yue, *The Handbook of Inorganic Metalloid Materials Atlas*, p. 280-364, Wuhan University of Technology Press (2000).
- L. H. Liu, R. J. Xie, N. Hirosaki, T. Takeda, J. G. Li, and X. D. Sun, *J. Am. Ceram. Soc.*, **92**, 2668 (2009).
- C. H. Huang, L. Y. Luo, and T. M. Chen, *J. Electrochem. Soc.*, **158**, J341 (2011).
- V. Sivakumar and U. V. Varadaraju, *J. Electrochem. Soc.*, **156**, J179 (2009).
- Y. Gong, Y. H. Wang, X. H. Xu, Y. Q. Li, and Z. Q. Jiang, *J. Electrochem. Soc.*, **156**, J295 (2009).
- X. F. Song, R. L. Fu, S. Agathopoulos, H. He, X. R. Zhao, and R. Li, *J. Electrochem. Soc.*, **157**, J34 (2010).
- V. Sivakumar and U. V. Varadaraju, *J. Electrochem. Soc.*, **154**, J167 (2007).
- U. G. Caldino, *J. Phys.: Condens. Matter*, **15**, 7127 (2003).
- L. J. Yin, X. Xu, L. Y. Hao, W. J. Xie, Y. F. Wang, L. X. Yang, and X. F. Yang, *Mater. Lett.*, **63**, 1511 (2009).
- R. Shannon, *Acta crystallogr. Sect. A. Cryst. Phys. Diffr. Theor. Gen.*, **32**, 751 (1976).
- C. Ronning, M. Dalmer, M. Uhrmacher, M. Restle, U. Vetter, L. Ziegeler, H. Hofsass, T. Gehrke, K. Jarrendahl, and R. F. Davis, *J. Appl. Phys.*, **87**, 2149 (2000).